
Article:
Dell, A., Krynkin, A., Horoshenkov, K. et al. (1 more author) (2023) Low frequency attenuation of acoustic waves in a perforated pipe. The Journal of the Acoustical Society of America, 153 (3). pp. 1791-1801. ISSN 0001-4966

https://doi.org/10.1121/10.0017644

Low frequency attenuation of acoustic waves in a perforated pipe

A. Dell, A. Krynkin, K. V. Horoshenkov, et al.

Citation: The Journal of the Acoustical Society of America **153**, 1791 (2023); doi: 10.1121/10.0017644
View online: https://doi.org/10.1121/10.0017644
View Table of Contents: https://asa.scitation.org/toc/jas/153/3
Published by the Acoustical Society of America

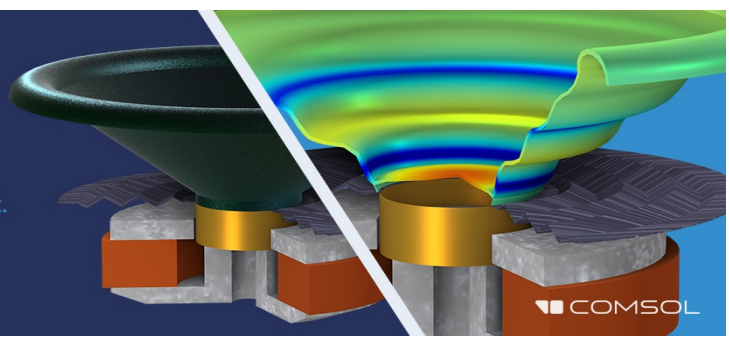

JASA ARTICLE

Low frequency attenuation of acoustic waves in a perforated pipe

A. Dell,[a] A. Krynkin, K. V. Horoshenkov, and G. Sailor
Department of Mechanical Engineering, The University of Sheffield, Sheffield, S1 3JD, United Kingdom

ABSTRACT:
This paper presents new experimental and numerical evidence that perforations in a pipe wall result in a low-frequency bandgap within which sound waves rapidly attenuate. These perforations are modelled as an acoustically soft boundary condition on the pipe wall and show that a low frequency bandgap is created from 0 Hz. The upper bound of this bandgap is determined by the dimensions and separation of the perforations. An analytical model based on the transfer matrix method is proposed. This model is validated against numerical predictions for the pipe with varying perforation geometries. A numerical study is undertaken to model the effect of perforations with ideal acoustically soft boundary conditions and surrounded with an air gap. Close agreement is found between the numerical and analytical models. Experimental evidence shows that the width of the bandgap is accurately predicted with the numerical and analytical models.
 https://doi.org/10.1121/10.0017644
(Received 23 November 2022; revised 25 February 2023; accepted 3 March 2023; published online 17 March 2023)
[Editor: Yong Li] Pages: 1791–1801

I. INTRODUCTION

The attenuation of acoustic waves in a pipe by silencers is typically achieved through the employment of rigidly backed cavities, connected to the pipe by a perforated panel. For silencers with partitioned cavities with a single perforation, i.e., a Helmholtz resonator, excellent attenuation can be achieved at the resonant frequency of the resonator. Multiple Helmholtz resonators can be side-loaded to the pipe, all tuned to different frequencies in order to achieve the broadband attenuation of noise.[1] Side-loaded Helmholtz resonators can be optimised to increase their absorptive performance by changing the separation distance between subsequent resonators and by adjusting their geometry and thus visco-thermal losses to critically couple them with the pipe. A similar technique has been employed in the design of sound absorbing acoustic metamaterials in order to achieve perfect broadband absorption in one and two port systems much smaller than the wavelength of the sound wave.[2,3]

For silencers with non-partitioned cavities and panels composed of multiple identical perforations along the length of the silencer a similar phenomenon occurs. If the perforated separating panel has a low porosity, a Helmholtz resonator type of attenuation occurs. As the porosity increases, the silencer behaves more like an expansion chamber.[4] Different configurations of partitions can be used to alter the number of resonances. Dissipative materials can be introduced to achieve broadband attenuation.[5] A limitation of these types of silencers is the requirement for large cavity volumes or narrow neck regions to achieve low frequency attenuation. A large cavity volume is often impractical and having narrow regions often results in poor attenuation of acoustic waves due to large amounts of visco-thermal losses often resulting in over-damping of the system.[6]

Through the use of a metamaterial consisting of an array of perforations along a waveguide, where no cavities are present, it has been theoretically and experimentally shown that negative bulk modulus can be obtained from zero to an upper bound.[7] This is due to the non-local resonant effect of the perforations allowing for the occurrence of a bandgap where zero transmission occurs and where the bandgap upper bound is determined by the system geometry. This has been corroborated in the non-linear regime through the employment of high amplitude excitation[8] and it has also been shown that through the coupling of the perforations within an array of elastic membranes, both negative bulk modulus and dynamic density can be achieved. Finally, it has been theoretically shown that in a sonic crystal in which the surfaces of each scatterer are modelled with an acoustically soft boundary condition, a bandgap is created from zero to an upper bound frequency determined by the surface area and periodicity of the soft scatterers.[9]

In this paper, an ideal analytical model is created to examine the influence periodic arrangements of sound-soft backed perforations have within a waveguide formed by an air-filled pipe. It is observed that the presence of periodically arranged soft scatterers results in a bandgap from 0 Hz to an upper bound. The upper bound of this bandgap is determined by the dimensions and separation of the perforations. Results are validated numerically with two modelling approaches employed to further refine the analytical model. Experimental evidence of a bandgap produced by acoustically soft scatterers is presented.

[a]Electronic mail: alexanderjdell1@gmail.com

This concept of acoustically soft scatterers much smaller than the wavelength enables us to achieve high attenuation at a very low frequency.

The paper is set out as follows: In the background theory section, an analytical model is derived using the transfer matrix method. This model is then used to assess the acoustic transmission loss (TL) of a pipe whose wall is comprised of periodic arrays of acoustically soft scatterers. Results from this analytical model are parametrically compared with those computed numerically for a variety of perforation geometries. This enables us to assess the relationship between variations in geometry and the width of the bandgap attained. Then, further numerical results are presented for a non-rigidly backed perforated pipe to understand better the acoustically soft boundary phenomenon occurring within the perforations. Finally, experimental results are presented and used to validate the numerical model.

II. BACKGROUND THEORY

A. Visco-thermal losses

The visco-thermal losses of an acoustic plane wave propagating in the fluid in a pipe wall perforation are accounted for by the complex frequency dependent density and bulk modulus.[10] For a circular duct of radius r that is much smaller than the wavelength λ,

$$\rho(\omega) = \rho_0\left[1 - \frac{2J_1(rG_r)}{rG_rJ_0(rG_r)}\right], \tag{1}$$

$$K(\omega) = K_0\left[1 + (\gamma - 1)\frac{2J_1(rG_k)}{rG_kJ_0(rG_k)}\right]. \tag{2}$$

Here, $G_r = \sqrt{-\mathrm{i}\omega\rho_0/\eta}$, $G_k = \sqrt{-\mathrm{i}\omega\rho_0 Pr/\eta}$, ρ_0 is the equilibrium fluid density, $K_0 = \gamma P_0$ is the adiabatic bulk modulus, γ is the ratio of specific heats, P_0 is the equilibrium pressure in the fluid, Pr is the Prandtl number, η is the fluid dynamic viscosity, ω is the circular frequency and $\mathrm{i} = \sqrt{-1}$. The harmonic time dependence is $\mathrm{e}^{\mathrm{i}\omega t}$ and is used throughout the paper. The effective dynamic fluid density and bulk modulus can then be used to obtain the characteristic impedance, $Z(\omega)$, and acoustic wavenumber, $k(\omega)$,

$$Z(\omega) = \frac{1}{S_a}\sqrt{\rho(\omega)K(\omega)}, \tag{3}$$

$$k(\omega) = \omega\sqrt{\frac{\rho(\omega)}{K(\omega)}}, \tag{4}$$

respectively.

B. The transfer matrix method (TMM)

The TMM provides the relationship between the initial sound pressure, p, and volume flux, $V = vS_a$, where S_a is the cross-sectional area and v is the acoustic particle velocity, at the start ($x = 0$) and at the end ($x = L$) of a medium in a rigid duct,[11] where L is the length of the medium. To differentiate between the initial and end properties of a medium in a duct, the subscripts 0 and L are used, respectively. The transfer matrix, T, is derived under the assumption that only plane waves propagate through the medium in the x direction, meaning it provides the solution for a one-dimensional (1D) wave propagation problem.[12]

The general formulation of the transfer matrix is as follows:

$$\begin{bmatrix} p \\ V \end{bmatrix}_{x=0} = T\begin{bmatrix} p \\ V \end{bmatrix}_{x=L} = \begin{bmatrix} T_{11} & T_{12} \\ T_{21} & T_{22} \end{bmatrix}\begin{bmatrix} p \\ V \end{bmatrix}_{x=L}. \tag{5}$$

The transfer matrix for a single fluid layer is constructed as

$$\begin{bmatrix} p \\ V \end{bmatrix}_{x=0} = \begin{bmatrix} \cos(kL) & \mathrm{i}Z\sin(kL) \\ \dfrac{\mathrm{i}}{Z}\sin(kL) & \cos(kL) \end{bmatrix}\begin{bmatrix} p \\ V \end{bmatrix}_{x=L} = \begin{bmatrix} T_{11} & T_{12} \\ T_{21} & T_{22} \end{bmatrix}\begin{bmatrix} p \\ V \end{bmatrix}_{x=L}. \tag{6}$$

Here, Z is the characteristic impedance and k is the acoustic wavenumber of the fluid, defined by Eqs. (3) and (4), respectively. For a multilayered structure, the relationship between the input and output pressure and acoustic flux is obtained by the multiplication of the transfer matrices of each layer,

$$T = \prod_{n=1}^{n_t} T^{(n)}, \tag{7}$$

where n_t denotes the total amount of layers.

III. IDEAL ANALYTICAL MODEL

A. Impedance of a perforation with soft boundary conditions

To determine the impedance of a single perforation of length d, characteristic impedance Z_p, and wavenumber k_p, with a soft boundary condition at depth $x = d$, the transfer matrix method is used. The full matrix, T, is derived from

$$T = M_{\Delta l}M_p, \tag{8}$$

where M_p models the cavity and is given by

$$M_p = \begin{bmatrix} \cos(k_pd) & \mathrm{i}Z_p\sin(k_pd) \\ \dfrac{\mathrm{i}}{Z_p}\sin(k_pd) & \cos(k_pd) \end{bmatrix}. \tag{9}$$

$M_{\Delta l}$ in Eq. (8) models the length correction due to pressure radiation at the interface between the perforation and the pipe, given by

$$M_{\Delta l} = \begin{bmatrix} 1 & \mathrm{i}Z_pk_p\Delta l \\ 0 & 1 \end{bmatrix}. \tag{10}$$

For a circular perforation, the length correction is[13]

https://doi.org/10.1121/10.0017644

$$\Delta l = 0.82\left[1 - 0.235\frac{r_p}{r_w} - 1.32\left(\frac{r_p}{r_w}\right)^2 + 1.54\left(\frac{r_p}{r_w}\right)^3 - 0.86\left(\frac{r_p}{r_w}\right)^4\right]r_p. \tag{11}$$

Here, r_w is the radius of the pipe (waveguide) and r_p is the radius of the perforation. To account for the acoustically soft boundary at the end of the perforation, the final T matrix is multiplied by $[0, 1]^T$, which provides a soft termination to the perforation at $x = d$ where acoustic volume flux is $V_{x=d}$ and pressure is $p_{x=d} = 0$. The characteristic impedance of the perforation with an acoustically soft boundary, Z_s, can then be found as

$$Z_s = \frac{P_{x=0}}{V_{x=0}} = \frac{T_{12}}{T_{22}} = \mathrm{i}Z_p \tan\left(k_p(d + \Delta l)\right). \tag{12}$$

B. Finite periodic system of sound soft scatterers

Consider a finite length of a pipe with n_t periodic arrangements of sound soft scatterers. Each unit cell has a length h and cross-sectional area S_w. The general geometry of the system can be seen in Fig. 1. The transfer matrix for the total system is given by

$$T = (M_w M_s M_w)^{n_t}. \tag{13}$$

M_w is the transfer matrix for a fluid layer of length $h/2$ and M_s is given by

$$M_s = \begin{bmatrix} 1 & 0 \\ N/Z_s & 1 \end{bmatrix}, \tag{14}$$

where N denotes the number of scatterers per unit cell. The total length of the system $L = n_{th}$. The TL of the total system can then be obtained as

$$TL = 20\log_{10}\left|\frac{T_{11} + T_{12}/Z + ZT_{21} + T_{22}}{2}\right|, \tag{15}$$

where Z is the characteristic impedance of the fluid within the pipe. As this system is symmetric and reciprocal, the transmission, reflection, and absorption coefficients can be determined as

$$T = \frac{2\mathrm{e}^{\mathrm{i}kL}}{T_{11} + T_{12}/Z + ZT_{21} + T_{22}}, \tag{16}$$

$$R = \frac{T_{11} + T_{12}/Z - ZT_{21} - T_{22}}{T_{11} + T_{12}/Z + ZT_{21} + T_{22}}, \tag{17}$$

$$\alpha = 1 - |R|^2 - |T|^2. \tag{18}$$

C. Bloch waves in an infinite periodic structure

Assuming plane wave propagation in a pipe with periodic imperfections, the Bloch Floquet theorem can be fulfilled so that the transfer matrix of a single unit cell can be described as follows:[14]

$$\begin{bmatrix} p \\ V \end{bmatrix}_{x=o} = T\begin{bmatrix} p \\ V \end{bmatrix}_{x=h} = \begin{bmatrix} T_{11} & T_{12} \\ T_{21} & T_{22} \end{bmatrix}\begin{bmatrix} p \\ V \end{bmatrix}_{x=h} = \begin{bmatrix} T_{11} & T_{12} \\ T_{21} & T_{22} \end{bmatrix}\begin{bmatrix} \mathrm{e}^{-\mathrm{i}qh}p \\ \mathrm{e}^{-\mathrm{i}qh}V \end{bmatrix}_{x=0}, \tag{19}$$

where q is the Bloch wavenumber. By rearranging, we obtain

$$\left(\begin{bmatrix} T_{11} & T_{12} \\ T_{21} & T_{22} \end{bmatrix} - \begin{bmatrix} \mathrm{e}^{\mathrm{i}qh} & 0 \\ 0 & \mathrm{e}^{\mathrm{i}qh} \end{bmatrix}\right)\begin{bmatrix} p \\ V \end{bmatrix}_{x=h} = 0. \tag{20}$$

By substituting $\Lambda = \mathrm{e}^{\mathrm{i}qh}$, the following eigenvalue problem can be constructed:

$$\begin{vmatrix} T_{11} - \Lambda & T_{12} \\ T_{21} & T_{22} - \Lambda \end{vmatrix} = \Lambda^2 - \Lambda(T_{11} + T_{12}) + |T| = 0. \tag{21}$$

In the previous equation, the determinant, $|T| = 1$, through the principle of reciprocity and therefore the forward and backward propagating Bloch waves display the same dispersion and the Bloch dispersion relation can be found as

$$\cos(qh) = \frac{1}{2}(T_{11} + T_{22}). \tag{22}$$

As such, the dispersion relationship for an infinitely periodic array of sound-soft backed perforations can be expressed as

$$\cos(qh) = \cos(kh) + \frac{\mathrm{i}ZN}{2Z_s}\sin(kh). \tag{23}$$

IV. IDEAL ANALYTICAL MODEL PARAMETRIC STUDY

In this section, a parametric study is undertaken where the relationship between the separation, depth and area of the perforations and the width of the bandgap produced is investigated. The analytical model is validated using three-dimensional (3D) numerical models in COMSOL Multiphysics 6.0.

Details of the selected geometries can be seen in Table I where the perforation radius is r_p, the perforation depth is d and the unit cell length is h. In all the cases the radius of the pipe, r_w, is 40 mm, the total number of unit cells, n_t, is 10 and the number of perforations per unit cell, N, is 6.

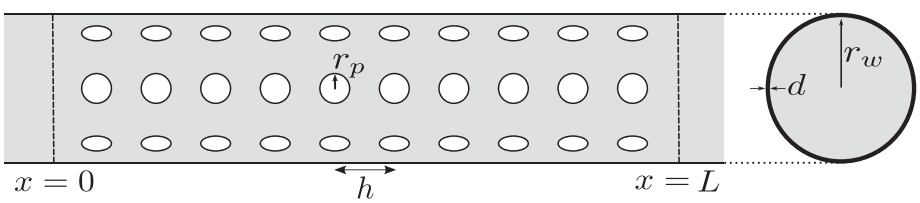

FIG. 1. Graphical representation of a finite system of sound soft scatterers.

TABLE I. Geometrical parameters of the four models validated numerically.

Geometry	r_p (mm)	d (mm)	h (mm)
1	2	5	50
2	2	5	25
3	3	5	50
4	2	10	50

These perforations are distributed evenly along the circumference of the pipe. Plots comparing the absorption, transmission and reflection coefficients predicted with the analytical and numerical model in the lossless and lossy cases can be seen in Fig. 2. In the lossless case, the effective fluid properties of the pipe and perforation are calculated with the lossless acoustic impedance and wavenumber such that visco-thermal losses are not taken into consideration. In

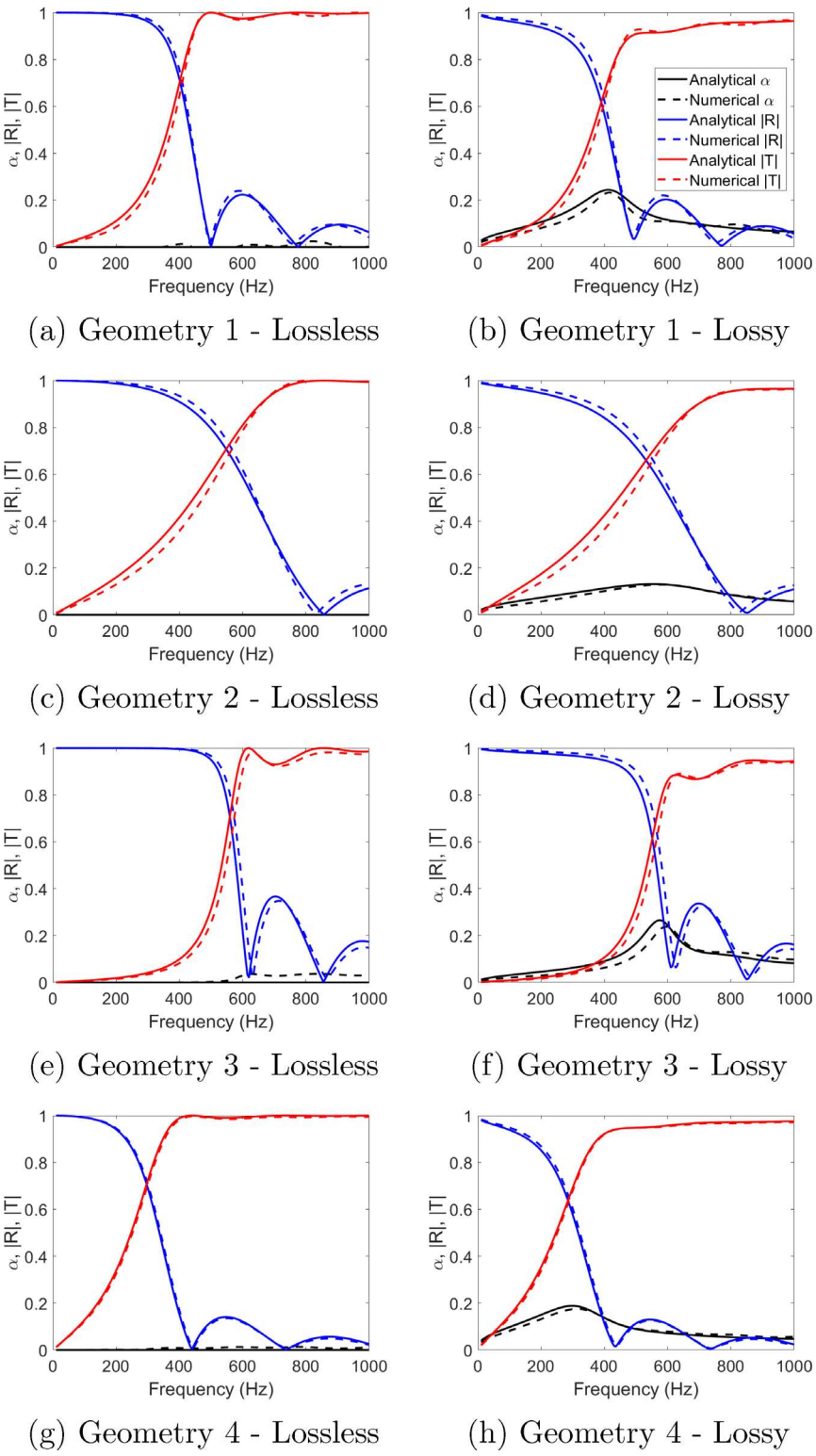

FIG. 2. (Color online) Analytical and numerical plots of α, $|R|$ and $|T|$ for Geometries 1–4 (Table II) in the lossless and lossy cases.

https://doi.org/10.1121/10.0017644

the lossy cases, all visco-thermal losses are included using Eqs. (1) and (2) to calculate the acoustic impedance and wavenumber. Plots of the TL predicted with analytical and numerical models and real and imaginary components of the Bloch wavenumber predicted with the analytical model are presented in Fig. 3. These results are also presented for the lossless and lossy cases. The results shown in Figs. 2 and 3 suggest that there is excellent agreement between the ideal analytical and 3D numerical models.

From Fig. 2(a), it is evident that in the lossless case, the introduction of acoustically soft backed perforations results in the reflection coefficient value close to unity at 0 Hz. This behaviour extends to approximately 300 Hz before the reflection coefficient begins returns to 0. Consequently, the

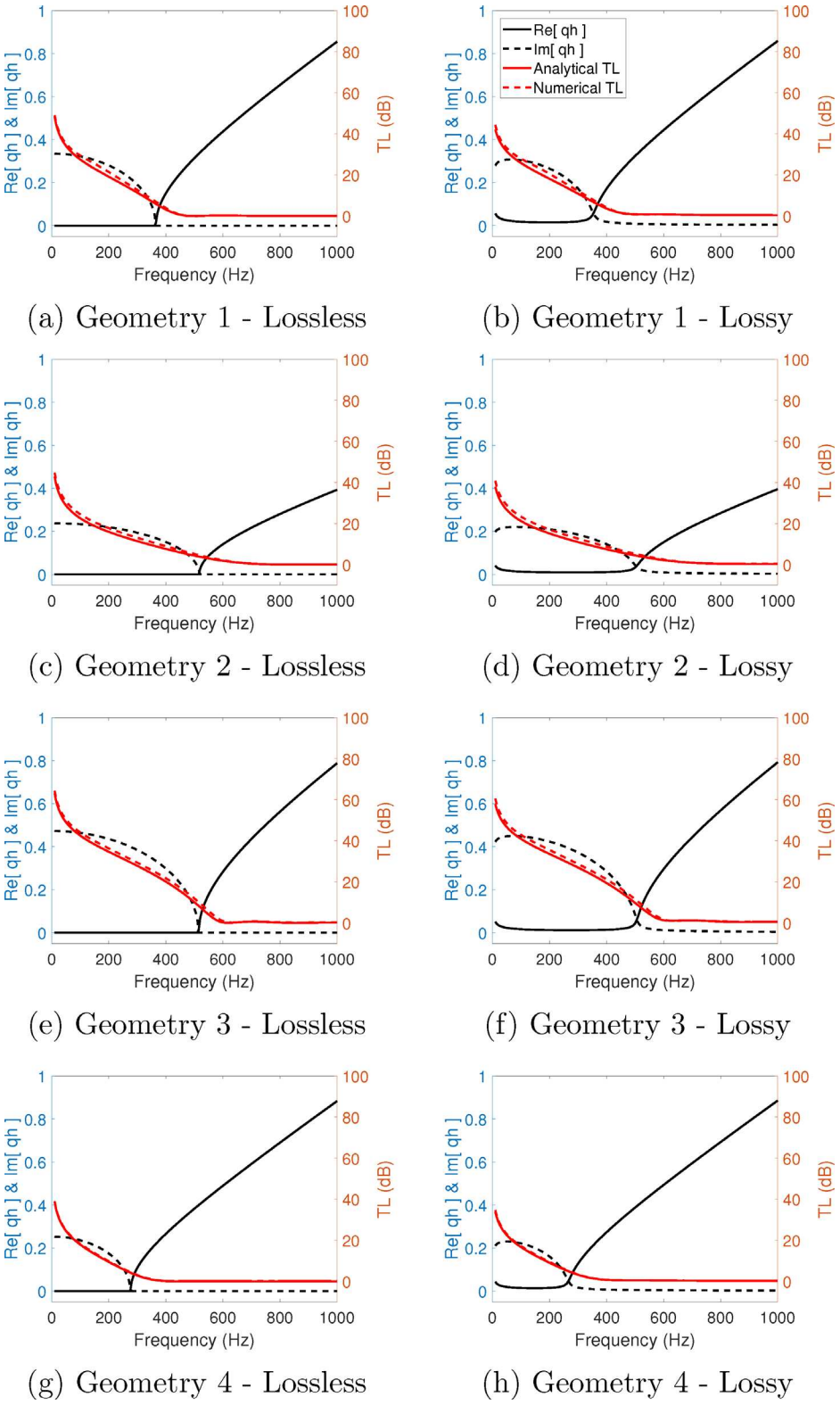

FIG. 3. (Color online) Analytical plots of the real and imaginary components of the Bloch wavenumber, and analytical and numerical plots of the TL for Geometries 1–4 (Table II) in the lossless and lossy cases.

transmission coefficient behaves in the opposite manner. This phenomenon is also clear in Fig. 2(b). In the lossless case there is no absorption present, whereas there is in the lossy case. Additionally, with losses the strength of the bandgap is reduced, with the reflection coefficient dropping from near unity immediately at frequencies above 0 Hz. There is no discernible change in TL.

In Fig. 3(a) a bandgap is evident, denoted by the purely imaginary Bloch wavenumber. This purely imaginary Bloch wavenumber indicates that the propagating wave within the bandgap frequency range is evanescent, which is evidenced by the TL across the same frequency range. It can be seen in Fig. 3(b) that the introduction of losses reduces the strength of the gap, with real values for the Bloch wavenumber occurring at 0 Hz.

In Geometry 2, the length of the unit cell has been halved, reducing the separation between the rows of perforations. Upon comparison of Fig. 2(c) with 2(a), it can be seen that by decreasing the unit cell length, the width of the bandgap is increased. It is worth noting that the reflection and transmission coefficients appear to change more gradually in this scenario. Again, as seen in Fig. 2(d), the introduction of losses induces absorption within the system. When looking at Figs. 3(c) and 3(d), the TL seems similar in amplitude to that predicted for Geometry 1, indicating that whilst the separation distance influences the width of the bandgap, it does not greatly impact TL.

To further investigate the relationship between the perforation geometry and the width of the bandgap produced, Geometry 3 is chosen to have the same geometrical parameters as Geometry 1, but an increase in perforation radius by 1 mm. When examining Figs. 2(e) and 2(f), the main difference to Geometry 1 is, an increase in the width of the bandgap. This time, the change in the reflection and transmission coefficients is similar to that produced by Geometry 1. From Figs. 3(e) and 3(f), it can be seen that by increasing the radius of the perforations it is possible to increase the width of the bandgap and amount of TL within the bandgap. This result indicates that the overall surface area of soft boundary conditions influences the TL produced by the perforations.

The final parameter is the depth of the perforation and how it influences the width of the bandgap produced. In Geometry 4, the depth of perforations is doubled, whilst the remaining parameters are kept consistent with Geometry 1. From Figs. 2(g) and 2(h), it can be seen that the width of the bandgap is reduced, with the reflection and transmission coefficients changing more gradually. In Figs. 3(g) and 3(h), it can be seen that by increasing the depth of the perforations, the TL is reduced in comparison to Geometry 1.

Therefore, for this system, it can be determined that the size and strength of the bandgap are dependent on multiple factors. Reducing the unit cell length, but keeping the total number of unit cells increases the width of the gap, but it does not increase the TL within the bandgap. Increasing the size of the perforation increases the surface area where a sound-soft boundary condition is present, which increases the size and TL of the bandgap. Finally, an increase in the perforation depth reduces the size and TL within the bandgap.

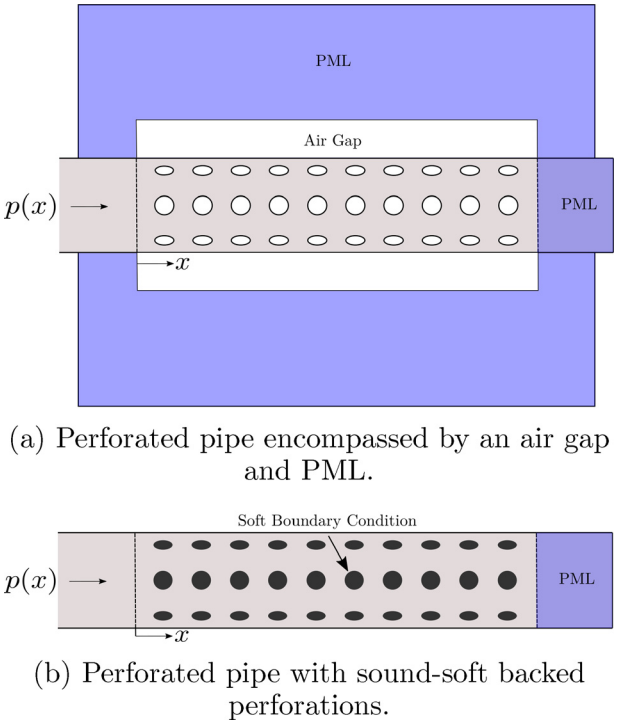

(a) Perforated pipe encompassed by an air gap and PML.

(b) Perforated pipe with sound-soft backed perforations.

FIG. 4. (Color online) Graphical representation of the numerically modelled perforated pipes with an air gap (a) and acoustically soft boundary (b).

V. NUMERICAL STUDY OF SOUND SOFT PHENOMENON

In this section, a numerical study is undertaken to further understand the acoustically soft boundary effect produced by non-rigidly backed perforations. To do this, two variants of numerical models are used which model the soft boundary condition differently. In the first variant, the perforations are encompassed by an air gap and then a perfectly matched layer (PML), whereas in the other variant, the outer boundary of the perforations is modelled with an ideal acoustically soft boundary condition. The PML is used to artificially attenuate any acoustic wave propagating away from the perforated pipe and minimise reflections back into the pipe from the boundary of the fluid domain surrounding the pipe.[15] Graphical representations of these two variants can be seen in Figs. 4(a) and 4(b),

TABLE II. The parameters of the three geometries of perforations used in the numerical model of the perforated pipe.

Geometry	r_p (mm)	d (mm)	h (mm)	n
1	5	5	50	11
2	5	5	25	21
3	2.5	5	25	21

https://doi.org/10.1121/10.0017644

respectively. Three perforation geometries and spacing are modelled with the parameters summarised in Table II. The radius of the pipe is kept constant between each model at $r_w = 40$ mm, and the number of perforations per unit cell is always $N = 1$. The transmission, reflection, and absorption coefficient spectra for Geometries 1–3 (see Table II) are shown in Fig. 5. These results are given for the perforated pipe surrounded with an air gap (dashed lines) and ideal acoustically soft boundary (solid lines). The behaviour of the absorption, reflection, and transmission coefficients shown in Fig. 5 suggests that the bandgap phenomenon cased by the perforations is present in both the variants of the numerical model. This is evidenced by the near unity reflection coefficient as the frequency reduces to 0 Hz. The width of the bandgap differs between the two variants of the numerical model. In the case of the model for the ideal acoustically soft boundary conditions, the high attenuation band extends over a larger frequency range for each of the three perforation geometries considered in this study. It can therefore be determined that an additional length correction due to pressure radiation at the soft boundary of the perforation is required. Additionally, in Figs. 5(a) and 5(b), it can be seen that the numerical results produced for the variant with the air gap and PML are noisy due to numerical artifacts resulting from the PML.

VI. REVISED ANALYTICAL MODEL

In order to account for the extra pressure radiation that occurs at the discontinuity from the perforation and the surrounding medium, an additional length correction to the perforation depth must be accounted for in the expression for the impedance of a perforation with a soft boundary condition. Equation (11) gives the length correction, Δl, for the pressure radiation at the discontinuity between the perforation and fluid within the perforated pipe. In addition to this, an expression of the length correction for the pressure radiation from an orifice in a tube wall into free space is required. This is given by the following equation:[16]

$$\Delta l_2 = \frac{U_p}{8} + k_0^{-1}\chi_0\left(2k_0\sqrt{\frac{S_p}{\pi}}\right), \tag{24}$$

where U_p is the perimeter of the perforation, $k_0 = \omega/c_0$, and

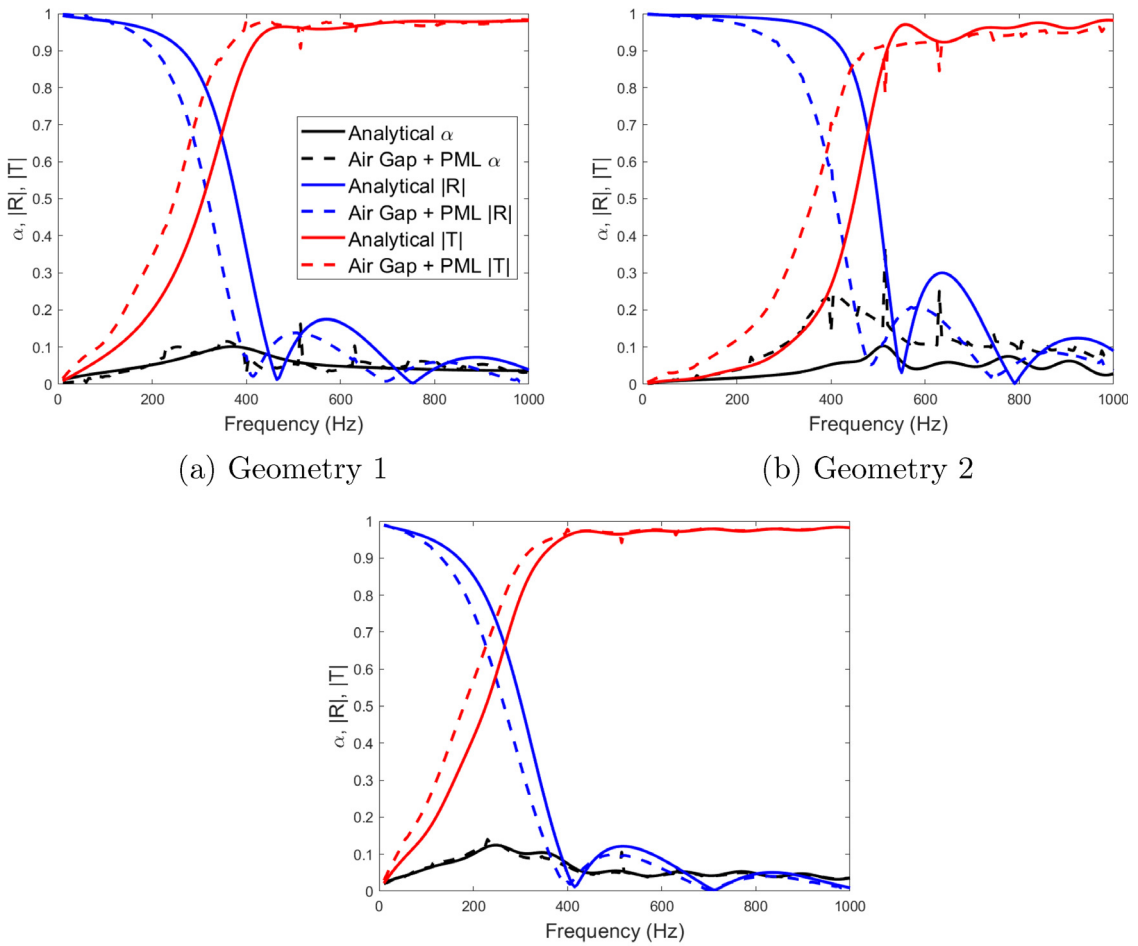

FIG. 5. (Color online) Plots of α, $|R|$ and $|T|$ for both numerical variants for Geometries 1–3 (Table II).

$$\chi_0(\xi) = \frac{4}{\pi}\int_0^{\pi} \sin(\xi\cos(a))\sin^2(a)\mathrm{d}a \approx \frac{\xi^2}{8} \quad \text{for} \quad \xi \ll 1. \tag{25}$$

Here, $\xi = 2k_0\sqrt{S_p/\pi}$. If the length correction for the pressure radiation at the discontinuity between the perforation and pipe is

$$\Delta l_1 = 0.82\left[1 - 0.235\frac{r_p}{r_w} - 1.32\left(\frac{r_p}{r_w}\right)^2 + 1.54\left(\frac{r_p}{r_w}\right)^3 - 0.86\left(\frac{r_p}{r_w}\right)^4\right]r_p, \tag{26}$$

as described in Eq. (11), then the equation for the revised impedance for a perforation with a sound soft boundary [see Eq. (12)] is

$$Z_s = \mathrm{i}Z_p\tan(k_p(d + \Delta l_1 + \Delta l_2)). \tag{27}$$

The methodology presented in Sec. III B and Eq. (27) was used to compare the revised analytical model against the numerical simulation detailed in Sec. V. The results of this comparison are shown in Fig. 6 for the three geometries presented in Table II. Figure 6 presents the absorption, reflection, and transmission coefficients for the perforated pipe encompassed by an air gap and PML. From these figures, it can be seen that there is now an excellent agreement between the revised analytical and numerical models suggesting that the revised analytical model now provides a simple and robust way to determine the acoustic attenuation in a pipe with non-rigidly backed circular perforations.

VII. EXPERIMENTAL RESULTS

In order to validate the proposed analytical and numerical models and to illustrate practically the existence of the low frequency bandgap, an experimental pipe rig was set up in the ICAIR laboratory at the University of Sheffield. The experimental rig included a 1.32 m perforated pipe with a smooth inner radius 0.8 m and a corrugated outer radius, with three perforations per cross section and approximately 1 m of separation between the speaker and

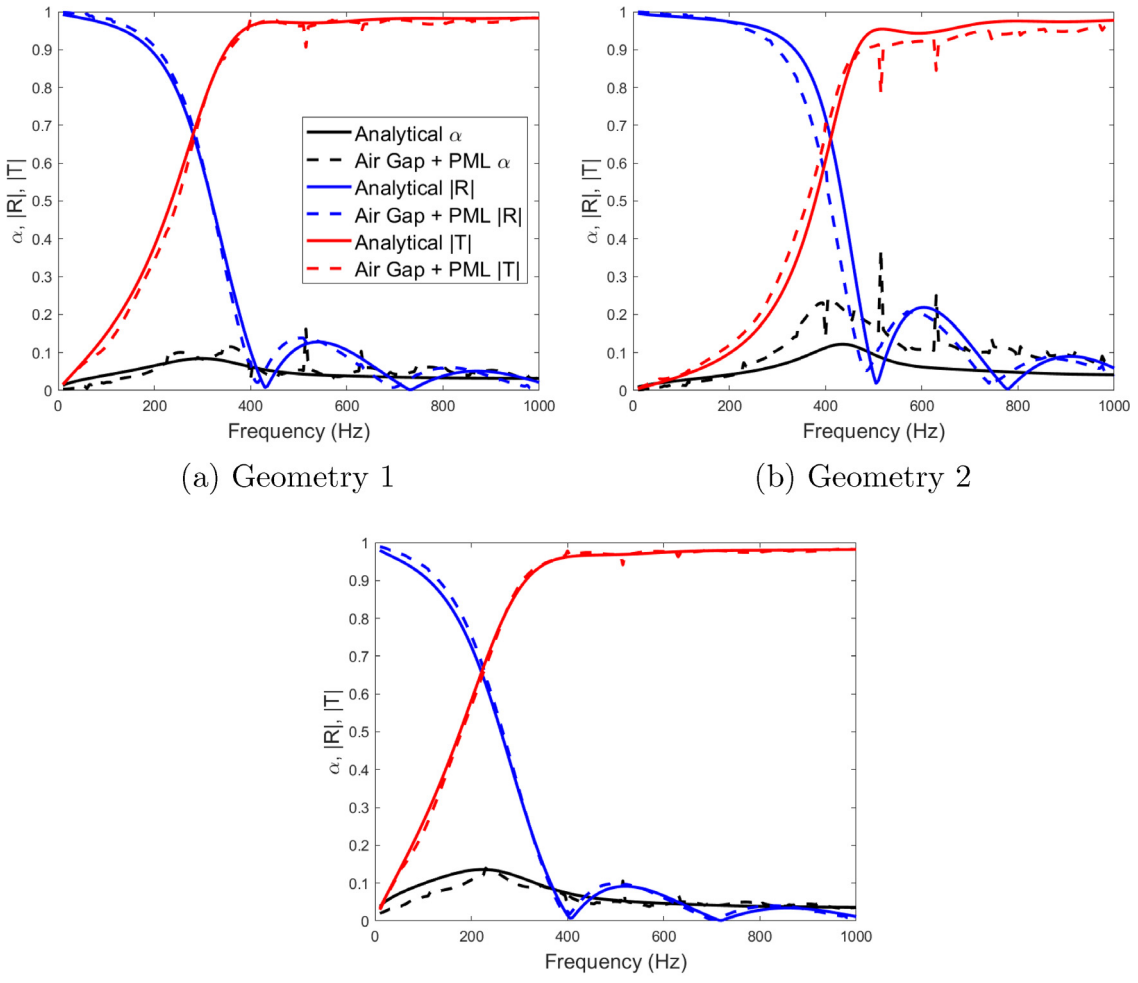

(a) Geometry 1 (b) Geometry 2

(c) Geometry 3

FIG. 6. (Color online) The spectra of the absorption, α, reflection, $|R|$, and transmission, $|T|$, coefficients predicted with the revised analytical model and numerical model for the pipe with the peroration geometries defined in Table II.

https://doi.org/10.1121/10.0017644

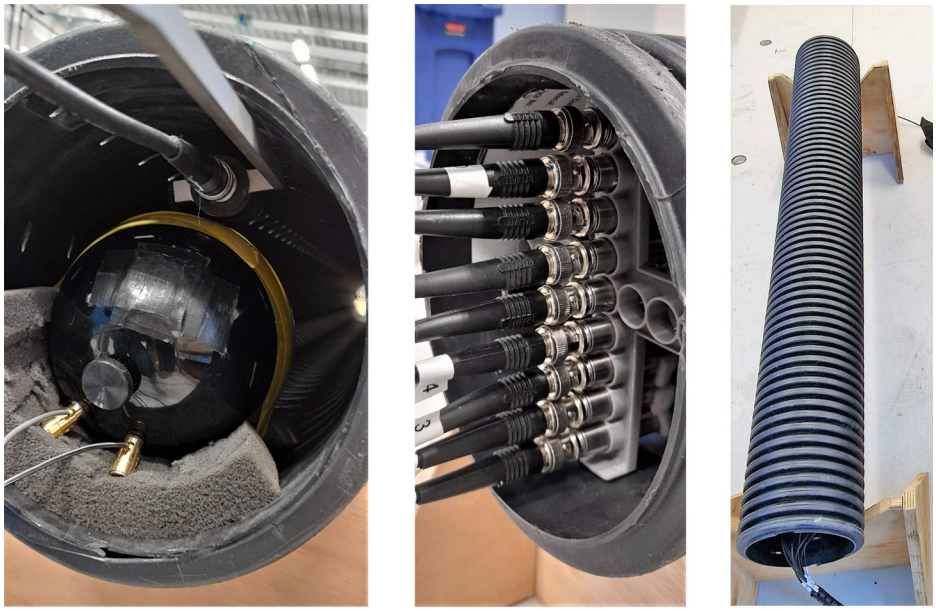

(a) (b) (c)

FIG. 7. (Color online) The experimental pipe set up at the ICAIR: (a) sound speaker at the source end; (b) array of nine microphones at the receiver end; (c) perforated pipe with speaker and microphone array installed at the opposite ends of the pipe.

an array of nine microphones as illustrated in Figs. 7(a)–7(c). The speaker was piston-on-a-sphere which is designed to act like a source with high radiation efficiency.[17] The speaker was installed at one end of the perforated pipe as shown in Fig. 7(a). The speaker was driven by a sine sweep generated between 50 Hz and 25 kHz with the help of a NI-9260 analog output module and B&K type 2716 °C amplifier.

The microphone array made of nine GRAS 46AE 1/2″ CCP free-field standard microphones (GRAS Sound and Vibration, Holte, Denmark) was installed at the other end of the pipe. It was arranged along the pipe diameter as shown in Fig. 7(b). The microphone array was used to filter out the plane wave mode in a sufficiently broad frequency range. It is noted that the locations of holes in the perforated pipe along the pipe circumference were not consistent and varied along the pipe length. The spacing between the rows of perforation was fixed at $h = 20$ mm and the width of each perforation was approximately 20 mm as shown in Figs. 8(a) and 8(b), respectively. A National Instrument data acquisition module type NI-9232 was used to acquire data at the sampling rate of 51.2 kHz. Figure 9 illustrates the TL obtained with the following equation:

$$TL = 20 \log_{10} \left| \frac{p_{ref}}{p_{rec}} \right|, \tag{28}$$

where p_{ref} is the acoustic pressure recorded at the reference microphone in the vicinity of the sound speaker and p_{rec} is the acoustic pressure recorded at the receiver side with the array microphones. The experimental pipe geometry was replicated in a 3D finite element method (FEM) model in

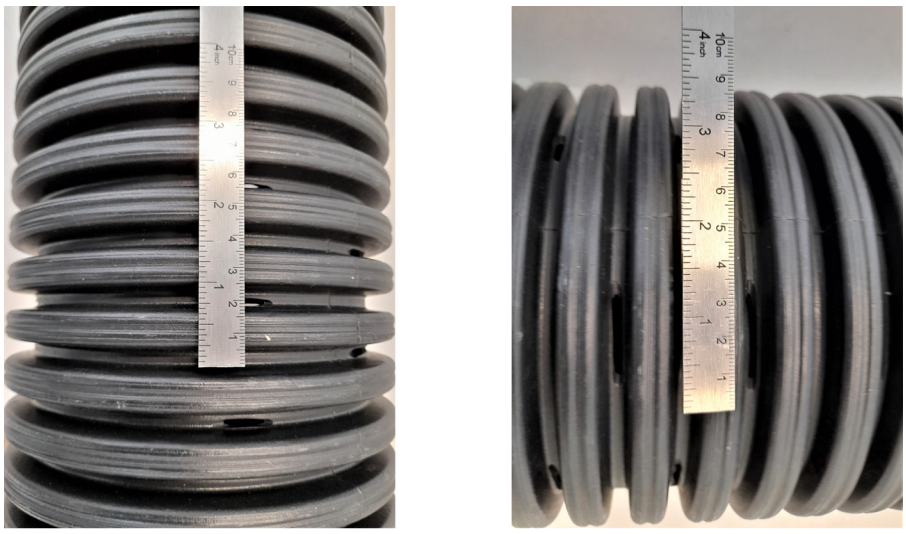

(a) (b)

FIG. 8. (Color online) Pipe perforation: (a) Axial distance between perforation; (b) width of a single perforation.

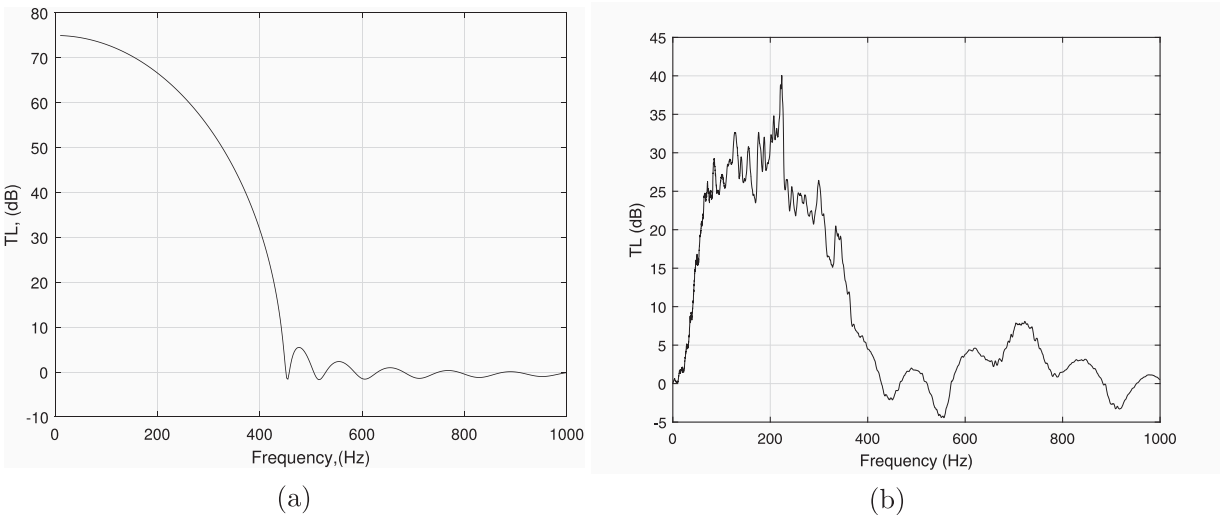

FIG. 9. The transmission loss [Eq. (28)] predicted with the numerical model (a) and measured using the proposed experimental rig (b).

COMSOL multiphysics 6.0 with ideal soft boundary conditions at the interface of the perforation and PML imposed at the end of the pipe away from the sound source. The sound source was modelled as a piston generating plane wave. The perforations were modelled as ellipses of constant cross-sectional area. The results of the numerically and experimentally obtained TL can be seen in Fig. 9. The measured TL illustrated in Fig. 9(b) offers evidence that the periodically arranged perforations in the rigid pipe create a low frequency bandgap that extends to approximately 460 Hz. The width of this bandgap matches that predicted for the simplified perforation geometry, i.e., where the perforations are idealised with an elliptical geometry in the 3D finite element model. It is evident, however, that the experimental data set is noisy and that the level of the experimental TL is limited by the signal-to-noise ratio. This difference can also be attributed to a structure-borne vibrations excited in the wall of the pipe or sound leakage due to the experimental perforated pipe being open-ended. Despite this, it can be seen that the acoustically soft scattering phenomenon discussed in Sec. II does occur when the pressure release condition is imposed on a non-rigidly backed perforation allowing for very low frequency attenuation of acoustic waves with a sample size much smaller than the wavelength of sound being attenuated.

VIII. CONCLUSIONS

An analytical model based upon the transfer matrix method has been developed to predict the acoustic attenuation in a pipe caused by a periodic array of non-rigidly backed perforations acting like acoustically soft scatterers. It has been shown that periodic arrays of acoustically soft scatterers produce a low frequency bandgap from 0 Hz to an upper bound determined by the geometry of the perforations and the unit cell length. Acoustic waves within the frequency range of the bandgap become evanescent causing a significant attenuation. As a result, there is no wave propagation in infinite pipe with perforation. Reducing the unit cell length, but keeping the total number of unit cells constant, increases the width of the gap, but does not increase the attenuation within the bandgap. Increasing the size of the perforation increases the surface area where an acoustically soft boundary condition is present. This causes an increase in the width of the bandgap and attenuation within it. Additionally, it is possible to adjust the width of the bandgap and attenuation by changing the depth of the perforations. An increase in the perforation depth results in a reduction in the width of the bandgap and attenuation achieved within it. All of these observations are numerically validated indicating in the ideal case the analytical model is valid. An experiment has been carried out to illustrate that the models predict the width of the bandgap.

ACKNOWLEDGMENTS

The authors are grateful for the financial support of the doctoral training grant provided by the Department of Mechanical Engineering at the University of Sheffield and the UK Engineering and Physical Sciences Research Council (EPSRC) Grant No. EP/N509735/1. A.D. is grateful for the financial support of Sonobex Ltd. ICAIR has been part funded by EPSRC, Grant UKCRIC-National Distributed Water Infrastructure Facility (EP/R010420/1) and the European Regional Development Fund (Project Number 28R15P00608). Parts of this work were supported by Innovate UK Grant 76593—Innovative Sensor Array for Sewer Survey. For the purpose of open access, the author has applied a "Creative Commons Attribution (CC BY)" licence to any Author Accepted Manuscript version arising.

[1]S.-H. Seo and Y.-H. Kim, "Silencer design by using array resonators for low-frequency band noise reduction," J. Acoust. Soc. Am. **118**(4), 2332–2338 (2005).
[2]N. Jiménez, V. Romero-García, V. Pagneux, and J.-P. Groby, "Quasiperfect absorption by subwavelength acoustic panels in transmission using accumulation of resonances due to slow sound," Phys. Rev. B **95**(1), 014205 (2017).

[3]N. Jiménez, V. Romero-García, V. Pagneux, and J.-P. Groby, "Rainbow-trapping absorbers: Broadband, perfect and asymmetric sound absorption by subwavelength panels for transmission problems," Sci. Rep. **7**(1), 13595 (2017).
[4]J. W. Sullivan and M. J. Crocker, "Analysis of concentric-tube resonators having unpartitioned cavities," J. Acoust. Soc. Am. **64**(1), 207–215 (1978).
[5]I. Lee, "Acoustic characteristics of perforated dissipative and hybrid silencers," Ph.D. thesis, The Ohio State University, Columbus, OH (2005).
[6]U. Ingard, "On the theory and design of acoustic resonators," J. Acoust. Soc. Am. **25**(6), 1037–1061 (1953).
[7]S. H. Lee, C. M. Park, Y. M. Seo, Z. G. Wang, and C. K. Kim, "Acoustic metamaterial with negative modulus," J. Phys.: Condens. Matter **21**(17), 175704 (2009).
[8]J. Zhang, V. Romero-García, G. Theocharis, O. Richoux, V. Achilleos, and D. J. Frantzeskakis, "Second-harmonic generation in acoustic waveguides loaded with an array of side holes," Acta Acust. united Ac. **104**(2), 235–242 (2018).
[9]A. Krynkin and P. McIver, "Approximations to wave propagation through a lattice of Dirichlet scatterers," Waves Random Complex Media **19**(2), 347–365 (2009).
[10]M. R. Stinson, "The propagation of plane sound waves in narrow and wide circular tubes, and generalization to uniform tubes of arbitrary cross-sectional shape," J. Acoust. Soc. Am. **89**(2), 550–558 (1991).
[11]N. Atalla and Jean F. Allard, *Propagation of Sound in Porous Media* (John Wiley & Sons, New York, 2009).
[12]A. Dell, A. Krynkin, and K. Horoshenkov, "The use of the transfer matrix method to predict the effective fluid properties of acoustical systems," Appl. Acoust. **182**, 108259 (2021).
[13]V. Dubos, J. Kergomard, A. Khettabi, J.-P. Dalmont, D. Keefe, and C. Nederveen, "Theory of sound propagation in a duct with a branched tube using modal decomposition," Acta Acust. united Ac. **85**, 153–169 (1999).
[14]C. E. Bradley, "Time harmonic acoustic Bloch wave propagation in periodic waveguides. Part I. theory," J. Acoust. Soc. Am. **96**(3), 1844–1853 (1994).
[15]Q.-H. Liu and J. Tao, "The perfectly matched layer for acoustic waves in absorptive media," J. Acoust. Soc. Am. **102**(4), 2072–2082 (1997).
[16]M. L. Munjal, F. P. Mechel, M. Vorländer, P. Költzsch, and M. Ochmann, *Formulas of Acoustics* (Springer, London, 2008).
[17]F. Jacobsen and V. Jaud, "A note on the calibration of pressure-velocity sound intensity probes," J. Acoust. Soc. Am. **120**(2), 830–837 (2006).